frontiers | Frontiers in Earth Science

TYPE Original Research
PUBLISHED 16 June 2023
DOI 10.3389/feart.2023.1084673

OPEN ACCESS

EDITED BY
Fan Yang,
Lanzhou University, China

REVIEWED BY
Jian Li,
Shandong University of Technology, China
Leilei Dong,
University of Science and Technology Beijing, China
Yong Wang,
Chengdu University of Technology, China

*CORRESPONDENCE
Haiqin Wang,
haiqinw@163.com

RECEIVED 30 October 2022
ACCEPTED 24 May 2023
PUBLISHED 16 June 2023

CITATION
Tian R, Wang H, Tian J, Shan W, Wang X, Chi N, Ma X, Chu Z, Li S and Lv Q (2023), Preliminary investigation of the eruption time of kimberlite in the Late Devonian in Mengyin, Shandong.
Front. Earth Sci. 11:1084673.
doi: 10.3389/feart.2023.1084673

Preliminary investigation of the eruption time of kimberlite in the Late Devonian in Mengyin, Shandong

Ruicong Tian[1], Haiqin Wang[2]*, Jingxiang Tian[2], Wei Shan[2], Xiufeng Wang[2], Naijie Chi[2], Xiaodong Ma[2], Zhiyuan Chu[3], Shenghu Li[2] and Qing Lv[3]

[1]School of Geography and Tourism, Qilu Normal University, Jinan, China, [2]Ministry of Natural Resources Key Laboratory of Gold Mineralization Processes and Resources Utilization, Shandong Key Laboratory of Metallogenic Processes and Resource Utilization of Metallic Minerals, Shandong Institute of Geological Sciences, Jinan, China, [3]The 7th Institute of Geology and Mineral Exploration of Shandong Province, Linyi, Shandong, China

Kimberlite in the Mengyin area serves as an excellent medium for studying the characteristics and evolutionary processes of the Paleozoic mantle. In order to determine the age of the primary calcite within the kimberlite, *in situ* carbonate U–Pb dating was conducted in the Mengyin area. The results indicate that the primary calcite in the kimberlite originated approximately 383 ± 18 Ma (MSWD = 6.6). This age constraint suggests that the eruption of the kimberlite took place during this period, leading to the thermal alteration of limestone xenoliths, ultimately forming marble. Consequently, it can be inferred that lithospheric thinning occurred no later than the Late Devonian period. Fluid inclusions found within the marble provide further insights into its formation. The recorded formation temperature of the marble ranges from 243°C to 370°C, with a salinity range of 2.57%–14.77% (NaCl). The pressure estimates fall within the range of 3.22–20.70 MPa, indicating a depth mainly between 900 and 1,000 m. Based on these findings, it can be inferred that the overall denudation depth in the west Shandong area, since the Late Devonian, is estimated to be approximately 900–1,000 m. Furthermore, the overall crustal rise rate is estimated to be approximately 3 m/Ma.

KEYWORDS

kimberlite, diamond, fluid inclusions, carbonate dating, plate subduction, Mengyin region

1 Introduction

Kimberlite, classified as alkaline mafic ultrabasic rocks, represents the deepest form of magma found in nature. It originates from the upper mantle, at depths ranging from 150 to 300 km, under high temperature and pressure (Heaman et al., 2003; Giuliani et al., 2016). Due to its unique origin, kimberlite carries valuable geological information, making it a vital channel for studying mantle compositions. Sheng (2004) characterized the metallogenic conditions of diamond deposits as follows: a thick upper mantle with low heat flow and high depletion beneath ancient cratons, which provides a favorable environment for the formation of kimberlite magma and the upward migration of diamonds. In addition, deep faults in the supercrustal region act as channels for the ascent of kimberlite. Lu et al. (1995) discovered that the crystallization processes of diamonds in the mantle exhibit a

prolonged time interval characterized by distinct stages. They further suggested that the magmatic activities of diamond-bearing kimberlite in eastern China were linked to the late Middle Ordovician continental uplift in the North China platform. According to Boyd et al. (1986), diamonds crystallize at the base of the lithosphere, with temperature and pressure being the primary controlling factors. Haggerty (1986) proposed that, in addition to temperature and pressure, oxygen fugacity also plays a significant role in diamond formation. During the extraction of mafic magma from the upper mantle, H_2O and CO_2 escape, resulting in a lithosphere that is not only compositionally depleted but also in a low oxidation state compared to the asthenosphere. Consequently, the interface between these two regions becomes the most favorable zone for diamond growth.

Kimberlite, which contains primary diamond ore deposits, was initially discovered in the Mengyin area of Shandong Province in 1965 (Liu, 2002; Wang et al., 2013; Wang and Wang, 2014; Wang et al., 2015). Since then, it has garnered significant attention, and numerous studies have extensively investigated its petrology, chronology, geochemistry, and its role in the evolution of the continental crust (Zhang, 2006; Zhang et al., 2007; Lu, 2010). Determining the precise formation age of the kimberlite in the Mengyin area has been a subject of debate. In the early 1980s, researchers from The 7th Institute of Geology and Mineral Exploration of Shandong Province discovered that the kimberlite vein intersected the diabase vein in the crystalline basement, with an isotopic age of 113 million years (Ma) at that time. Combining this with the 77–88 Ma obtained through K–Ar dating of the entire kimberlite, it was initially considered to be a product of the Cretaceous period in the Mesozoic era. In the following years, further investigations provided additional insights into the formation age of the kimberlite in the Mengyin area. Ion probe U–Pb analysis of perovskite yielded an age of 457 ± 7 Ma (Lu et al., 1995). This finding led to the proposal that the formation of diamonds occurred during the Paleozoic era, specifically in the Ordovician period, rather than in the Mesozoic era. Subsequent studies generated more Paleozoic age data, primarily concentrated in the range of 455–481 Ma, with the majority of model ages pointing toward the Ordovician period. Accurately constraining the formation age of the kimberlite remains a challenge in geochronological investigations. This is primarily due to the presence of extensive heterologous breccias within the kimberlite and the potential influence of late-stage alteration. These factors contribute to the complexities and uncertainties encountered when determining the precise age of the kimberlite formation.

The isotopic model age of perovskite in the Mengyin kimberlite was determined through U–Pb analysis, yielding a constraint of 465 ± 8 Ma (Song et al., 2009). Similarly, Yang et al. (2009) employed the U–Pb method to measure the isotopic model age of perovskite in the Mengyin kimberlite, resulting in a constraint of 470 ± 4 Ma. Phlogopite megacrysts collected from the Shengli No. 1 kimberlite pipe in the Changmazhuang rock belt were subjected to ^{39}Ar–^{40}Ar dating, yielding a plateau age of 466.3 ± 3 Ma and an isochron age of 464.9 ± 2.7 Ma. These ages align closely with the plateau age of 463.9 ± 0.9 Ma and isochron age of 463.9 ± 6.3 Ma obtained from phlogopite megacrysts in the No. 50 kimberlite pipe in Fuxian, Liaoning Province (Yang et al., 2009). Zhang et al. (2007) proposed that both Mengyin and Fuxian kimberlites were intruded at 465 Ma.

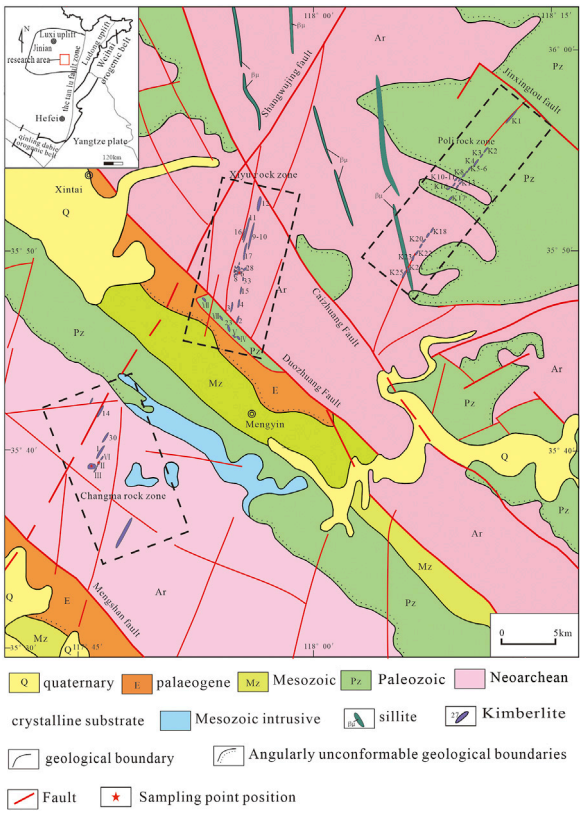

FIGURE 1
Geological map of kimberlite distribution in the Mengyin area (Lv and Ge, 2016). 1: Quaternary; 2: Paleogene; 3: Mesozoic; 4: Paleozoic; 5: Neoarchean crystalline substrate; 6: Mesozoic intrusive; 7: sillite; 8: kimberlite; 9: geological boundary; 10: angularly unconformable geological boundaries; 11: fault.

In a comprehensive study conducted by Li et al. (2016), multi-method tests were conducted on kimberlites taken from the Mengyin and Fuxian areas. Single-grain mica Rb–Sr isochron analysis and perovskite and baddeleyite ion probe U–Pb methods were utilized. The results indicated that the kimberlites in both areas were contemporaneous and formed 480 ± 3 Ma. By analyzing the results from different institutions, minerals, and analytical methods, Li et al. (2016) concluded that the intrusion ages of the kimberlite in the Mengyin area were likely constrained to the range of 450–460 Ma.

Kimberlite magma, originating from depths of approximately 200 km in the mantle, represents the deepest form of magma found in nature. It contains a wealth of deep geological information (Zhou et al., 2007) and serves as a crucial window for investigating the Earth's interior. Among the various components found within kimberlite, the xenoliths derived from the mantle are the most abundant. These xenoliths primarily consist of garnet peridotite, spinel peridotite, and dunite, as well as various types of pyroxene, eclogites, and metasomatic rocks (Lu et al., 1998; Lu, 2008). The age of kimberlite intrusion can be inferred from the thermal alteration of limestone breccias often found in brecciated kimberlite. These breccias undergo thermal alteration by the kimberlite magma, resulting in the formation of marble. In this study, we investigate

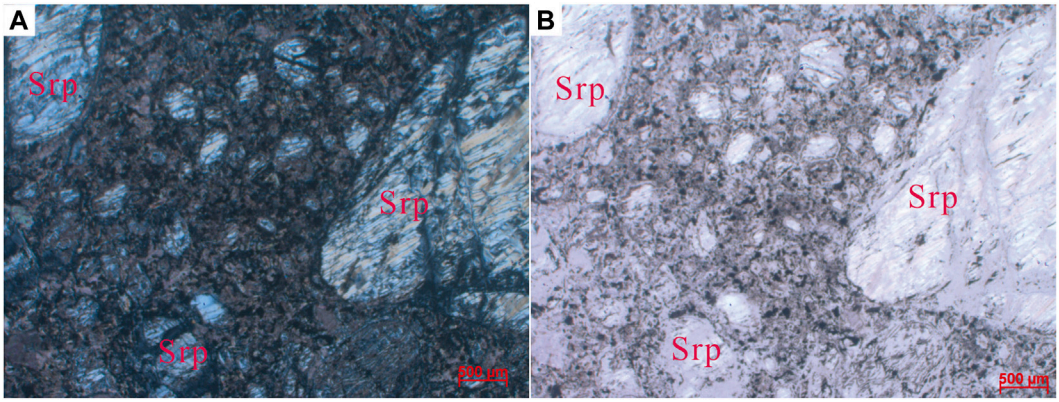

FIGURE 2
Photomicrographs of carbonatized-serpentinized kimberlite from Changmazhuang. **(A)** cross-polarized light photo; **(B)** plane-polarized photo. Srp-serpentine.

the pressure–temperature (P/T) conditions and the timing of the final consolidation of kimberlite at lower temperatures. This is achieved through the examination of fluid inclusions and U–Pb isotopic ages in calcite obtained from the kimberlite matrix and xenolithic marble, respectively.

2 Geological background

The kimberlite belt investigated in this study is situated in the eastern part of the North China Craton within the central Shandong uplift. It is bordered by the east Shandong uplift and the Sulu ultra-high pressure (UHP) metamorphic belt to the east, the Cenozoic Bohai Bay Basin to the north, and the Cenozoic Jining depression to the west. The geological composition of the area primarily comprises a Neoarchean crystalline basement consisting of metamorphic intrusive rocks, Paleozoic marine sedimentary cover, and Meso-Cenozoic continental basin sedimentary strata. Additionally, there are minor occurrences of Mesozoic diorite intrusive rock masses (Song et al., 2020). The Shangwujing fault, NW Mengshan fault, Xintai–Duozhuang fault, and Tongyedian–Sunzu fault are the major fault structures in the region (Figure 1).

The kimberlite belts in the Mengyin area are distributed across the Changmazhuang, Xiyu, and Poli regions (Figure 1). The overall orientation of these three kimberlite belts is approximately 55°, with a combined length of approximately 55 km and a width of 15 km. Each individual belt has a length of 12–15 km, gradually curving northeastward from south to north, resulting in a "broom" shape in their planar morphology as they scatter toward the north. The Changma rock belt is located in the southern region and consists of concentrated pipe distributions. The Xiyu rock belt is primarily controlled by two NNE-trending tectonic fracture zones, exhibiting a significant number of distributed pipes, with a predominant concentration around Xiyu. The Poli rock belt, situated in the northeastern area, displays a parallel intermittent distribution of single veins. The orientation of the individual veins within the rock belt remains consistent with each other. The diamond content in these three rock belts gradually decreases from south to north (Luo et al., 1999; Wang et al., 2015; Zhao, 2019), with the Poli kimberlite belt showing little or no presence of diamonds. Each vein is composed of numerous small veinlets arranged in a plume-like pattern, ranging in length from a few hundred meters to approximately 1,500 m. The individual veinlets within the veins generally exhibit a monomeric orientation of 20°–30°, tending toward the southwest or northwest with a steep dip.

The Changmazhuang rock belt is situated in the southern part of the Mengyin kimberlite area and comprises a total of two rock pipes and 113 single veins. The dense distribution of single veins allows for their subdivision into eight vein groups. The rock belt stretches over a length of 14 km and has a width of approximately 2.5 km (Zhang, 2006; Wang et al., 2013; Chen et al., 2018; Yang et al., 2018; Chu, 2019). The predominant lithologies within the Changmazhuang rock belt are porphyritic kimberlite, accompanied by carbonated-serpentinized kimberlite. These rocks exhibit a porphyritic texture as well as a massive structure. The mineral composition of the rocks is largely composed of olivine, garnet, phlogopite, calcite, opaque minerals, and other minerals (Figure 2).

The Xiyu rock belt is situated in the central part of the Mengyin kimberlite area and encompasses a total of 10 rock pipes and 11 groups of veins, consisting of 151 single veins. It stretches over a length of 15 km and has a width ranging from 0.5 km to 1 km (Chu, 2019). The overall strike of the rock belt is approximately 15°. The surrounding rocks in the area mainly consist of Neoarchean monzonitic granitic gneisses and early Paleozoic Cambrian–Ordovician sedimentary covers. The highest level of kimberlite intrusion is observed in the Wuyangshan Formation of the Middle Ordovician Majiagou Group. The major lithologies within the veins of the Xiyu rock belt predominantly exhibit phlogopite porphyritic kimberlite. At the northern end of the veins, there is a strong presence of limonitization and silicification. The veins oriented in the northwest direction display carbonated porphyritic kimberlite and fine porphyritic microporphyritic kimberlite (porphyrite) containing limestone or granitic breccia. The rock pipes within the belt are primarily composed of porphyritic kimberlite, followed by kimberlite breccia, porphyritic pyrope-kimberlite, fine-grained kimberlite, carbonated kimberlite, and porphyritic rock ball-bearing kimberlite, among others (Figure 3).

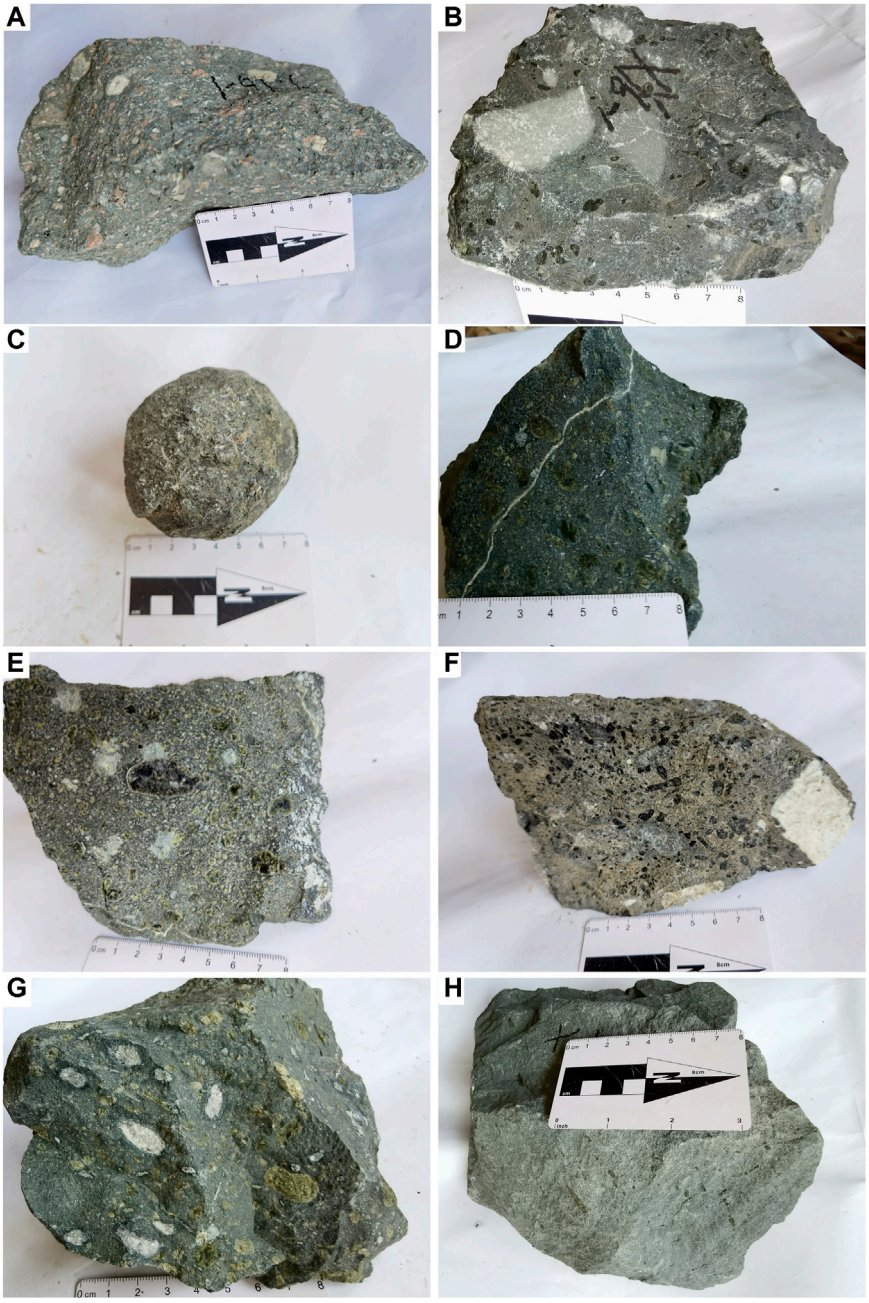

FIGURE 3
Various types of kimberlite from Xiyu. **(A)** Granitic kimberlite breccia. **(B)** Marbled kimberlite. **(C)** Kimberlite rock ball. **(D, E)** Porphyritic kimberlite containing pyrope. Porphyritic kimberlite containing pyrope. **(F, G)** Porphyritic kimberlite. Porphyritic kimberlite. **(H)** Fine-grained kimberlite.

The Poli rock belt is situated in the northern part of the Mengyin kimberlite area, with a general strike ranging from 35° to 40°. It comprises a total of 25 veins, with four groups consisting of 2–8 veins each (Chu, 2019). The prevailing lithology within the belt is finely porphyritic, microgranular phlogopite-bearing kimberlite, with the northern section, which is generated in the sedimentary cover, exhibiting a stronger degree of carbonation (Jin et al., 1999). The surrounding rocks invaded by the veins primarily consist of Neoarchean monzonitic granitic gneisses and Cambrian–Ordovician sedimentary covers (Du et al., 2019).

In terms of the diamond grade, the Changmazhuang rock belt generally exhibits a high grade and the Xiyu rock belt shows a medium grade, while the Poli rock belt presents a lower grade. This indicates a gradual decrease in diamond grade from south to north in the spatial–temporal distribution. In the first two rock belts, the mineralization of the rock pipes is generally higher than that of the veins, and it gradually depletes toward the deeper part. Based on the classification of magmatic stage minerals, hydrothermal alteration minerals, and xenolith minerals, the mineral assemblages of kimberlite in the Mengyin area can be divided into primary minerals, altered metasomatic minerals, and xenoliths (Table 1).

TABLE 1 Mineral assemblages of kimberlite in the Mengyin region.

Primary mineral (magmatic stage mineral)	Altered metasomatic mineral (minerals of hydrothermal alteration)	Xenolith mineral	
		Deep source	Generally surrounding rock
Olivine, phlogopite, pyrope, chrome spinel, diamond, chrome (green) diopside, picroilmenite, ilmenite, apatite, perovskite, yimengite, mathiasite, moissanite, graphite	Serpentine, bornite, calcite, sphalerite, talc, galena, chlorite, pyrite, titanite, millerite, hydromuscovite, magnetite, vermiculite, diopside, perovskite, covellite, leucoxene, malachite, hematite, chalcopyrite, limonite, pyrolusite, barite, andradite, grossular, uvarovite, phlogopite	Olivine, phlogopite, pyrope, chromitehrome (green) diopside, picroilmenite, diamond orthopyroxene, graphite	Pyrope–almandine, pyrope, tourmaline, hornblende, biotite, zircon, hematite, imonite, magnetite, rutile, anatase, quartz, feldspar, apatite

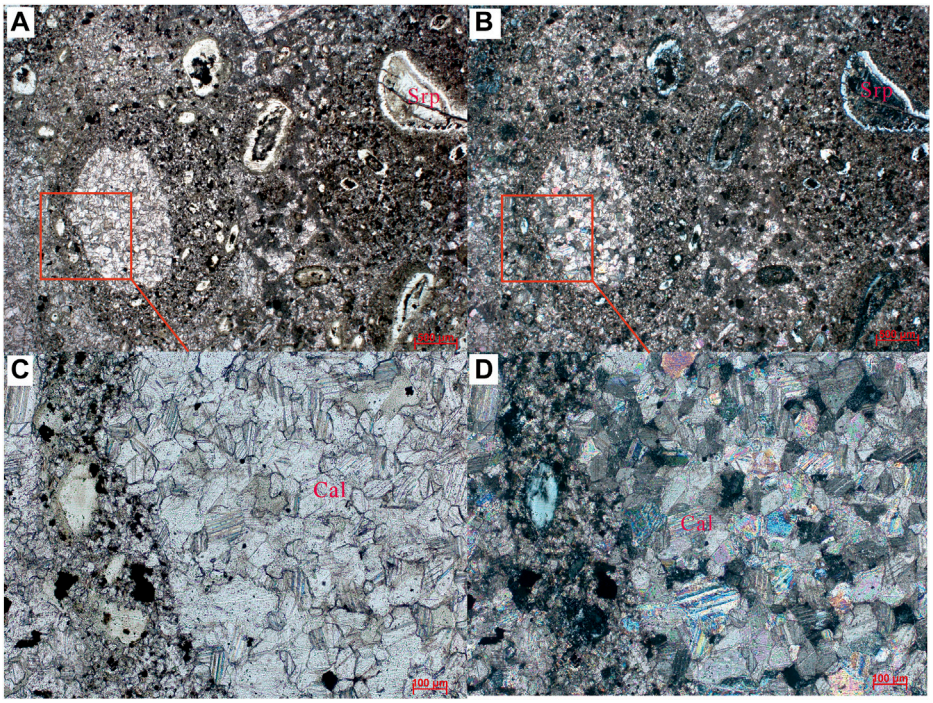

FIGURE 4
Characteristics of marble inclusions in kimberlite. **(A)** Plane-polarized light; **(B)** perpendicular polarized light; **(C)** partial of plane-polarized light; **(D)** partial of perpendicular polarized light. Srp, serpentine; Cal, calcite.

3 Sampling and analytical methods

3.1 Sampling

The samples were primarily collected from the rocks of the Changmazhuang, Xiyu, and Poli kimberlite belts in the Mengyin area, with a particular emphasis on the kimberlite-containing marble xenoliths in the Xiyu rock belt.

3.2 Analytical methods

In this study, several analytical procedures were conducted, including petrographic study using thin rock sections for identification, measurement of fluid inclusion temperatures, and U–Pb dating of carbonates.

The petrographic study and fluid inclusion temperature measurement were carried out at the Key Laboratory of Gold Mineralization Processes and Resource Utilization, affiliated with the Ministry of Land and Resources, and the Key Laboratory of Metallogenic Geological Process and Resources Utilization in Shandong Province. The fluid inclusions' homogenization and freezing temperatures were determined using a Linkam THMS600 hot and cold platform, manufactured in the United Kingdom, with temperature intervals ranging from −196°C to +600°C.

For carbonate U–Pb isotope age dating, calcite samples were collected from marble inclusions and kimberlite matrix in the Xiyu kimberlite. The marble was formed through the thermal alteration of limestone surrounding the kimberlite (Figure 4), providing information on the timing of the kimberlite diagenesis. *In situ* U–Pb dating was conducted using a laser-ablation microprobe at

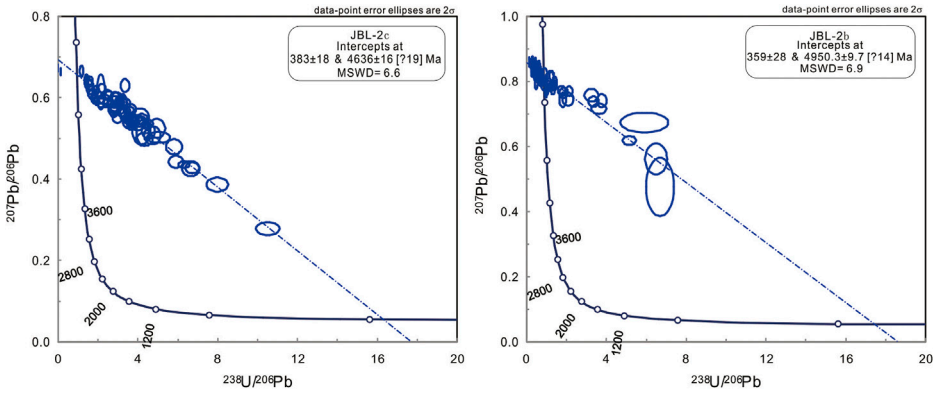

FIGURE 5
U–Pb concordia plot of carbonate in Xiyu kimberlite. JBL-2b, marble inclusions; JBL-2C, matrix calcite.

the Radioisotope Laboratory, University of Queensland. The sample was prepared as a 2.5-cm-diameter target and placed in a Laurin Technic cuvette. The ASI RESOlution SE laser-ablation system was coupled with a Thermo iCAP-RQ four-stage rod ICP-MS for ion scanning of ^{206}Pb, ^{207}Pb, ^{208}Pb, ^{238}U, and ^{232}Th. The laser-ablation frequency was set at 10 Hz, with a density of 3 J/cm^2, resulting in a laser ablation pit diameter of approximately 100 μm.

Sample processing involved the use of the international standard NIST-614 for isotope fractionation and offset correction of instrument sensitivity. U–Pb age correction was performed using calcite standards AHX-1D (203.3 ± 2.3 Ma), WC01-A (252.9 ± 1.8 Ma), and PTKD-2A (151.3 ± 6.0 Ma). The lower intercept ages were calculated using the Excel-loaded term Tera–Wasserburg of Isoplot (Paton et al., 2011) to obtain the U–Pb age of calcite (Yang et al., 2021).

3.3 Results

3.3.1 Results of carbonate U–Pb dating

The marble xenoliths can be observed as white masses within the kimberlite (Figure 4). In sample area b, the marble exhibits an average U content of 0.327×10^{-6} and a Pb content of 1.158×10^{-6} in calcite. On the other hand, the calcite in the matrix of area c shows an average U content of 4.618×10^{-6} and a Pb content of 4.468×10^{-6}. The Tera–Wasserburg diagram reveals a significant number of data points clustering around the upper intercept. Despite this, the resulting lower intercept ages of 359 ± 28 Ma (MSWD=6.9) and 383 ± 18 Ma (MSWD=6.6) remain reliable (Figure 5). The higher U and Pb contents in area c suggest less error and greater reliability in the data, which can be interpreted as the ages of primary calcite in the marble and kimberlite, respectively. Therefore, the formation time of the kimberlite can be constrained to 383 ± 18 Ma, while the marbleization process occurred slightly later, approximately 359 ± 28 Ma.

3.3.2 Petrographic characteristics and microthermometry of fluid inclusions

The Mengyin area showcases a diverse range of kimberlite types, including carbonated kimberlite, which contains a significant amount of recrystallized calcite and primary calcite particles. Within the calcite, both single-phase and two-phase fluid inclusions of varying sizes and quantities are present. For our current investigation, we collected fresh samples of carbonated kimberlite from the Mengyin area. These samples were prepared as double-polished microtonalite sheets, allowing for microscopic observation and subsequent microthermometry analysis.

3.3.2.1 Petrographic characteristics of fluid inclusions

Fluid inclusions within carbonated kimberlites are relatively scarce and not well-developed. Microscopic observation reveals the presence of three types of inclusions: single-phase liquid inclusions (type Ia, Figure 6A), single-phase gas inclusions (type Ib, Figure 6B), and water–gas–liquid two-phase inclusions (type II, Figures 6C–L). Among these types, the water–gas–liquid two-phase inclusions are more abundant than the single-phase inclusions. The inclusions can be found isolated, scattered, or clustered within calcite particles (Figures 6C–L). The individual inclusions are generally small, with most ranging from 2–8 μm, although some may exceed 10 μm in size (Figures 6C–F). In terms of shape, the inclusions typically exhibit a negative crystal shape of calcite (Figure 6G), columnar shape (Figures 6F, H), spherical shape (Figures 6D, I, J), oval shape (Figures 6K, L), and irregular shape (Figures 6C, E). The gas–liquid ratio of the majority of the two-phase inclusions is approximately 20%, while some bubbles within the two-phase inclusions with smaller gas–liquid ratios exhibit constant movement. Individual inclusions with larger gas–liquid ratios account for approximately 40% (Figures 6F, J).

3.3.2.2 Microthermometry of fluid inclusions

Given that the size of the single-phase inclusions was found to be smaller than 2 μm, only the microthermometry analysis of the aqueous two-phase inclusions was performed in this temperature measurement experiment.

During the analysis, the gas–liquid two-phase inclusions were homogenized into the liquid phase, and the homogenization temperature ranged from 243°C to 370°C. The freezing point temperature, which corresponds to the final melting temperature of water ice, varied between −10.8 and −1.5°C.

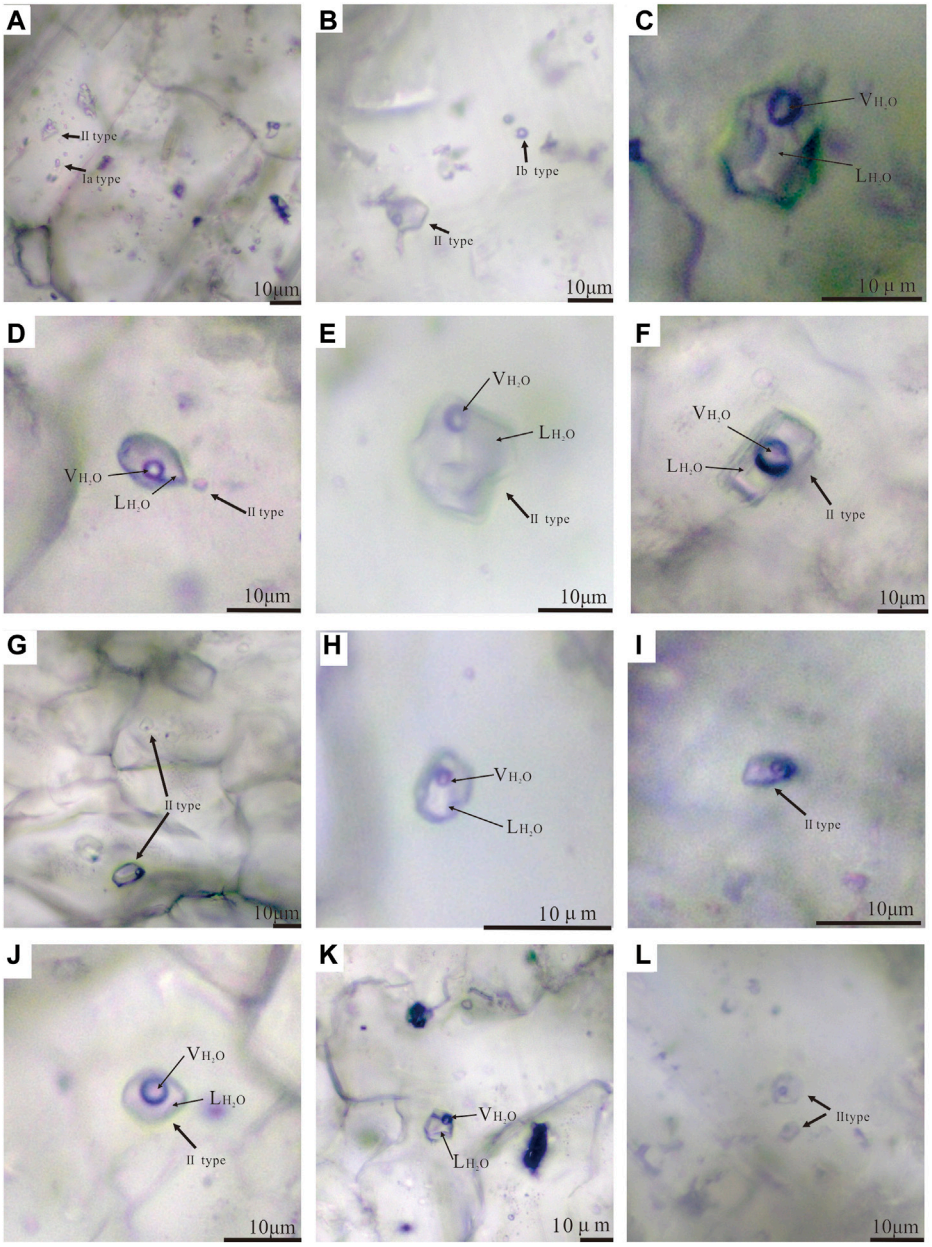

FIGURE 6
Photomicrographs showing representative examples of calcite-hosted fluid inclusions within the Mengyin kimberlites. **(A, B)** Ia Type and II Type fluid inclusions. **(C–F)** fluid inclusions exceed 10 μm in size. **(G)** inclusions exhibit a negative crystal shape of calcite. **(F, H)** columnar shape fluid inclusions. **(D, I ,J)** spherical shape fluid inclusions. **(K, L)** oval shape fluid inclusions. **(C, E)** irregular shape fluid inclusions. **(F, J)** Type II inclusions containing ~40% vapor phase. Abbreviations: V, vapor; L, liquid.

3.3.2.3 Physical and chemical parameters of the fluid inclusions

Based on the temperature measurement results of fluid inclusions, the complete homogenization temperature (Th-$_{TOT}$, ˚C) and freezing point (Tm-ice, ˚C) of fluid inclusions can be derived directly.

The salinity of gas–liquid two-phase inclusions was estimated using the salinity equation proposed by Potter et al. (1978), which utilizes the freezing point temperature (Tm-ice, ˚C), which is given as follows:

$S = 0.00 + 1.78 \times Ti\text{-}0.0442 \times Ti^2 + 0.000557 \times Ti^3$ (where Ti represents freezing point temperature).

When the salinity S is between 1% and 30%, the density of the brine solution in the inclusions can be obtained using formulas proposed by Haas (1970) and Bodnar (1983): $\rho = A + B \times t + C \times t^2$.

Here, ρ—brine solution density (g/cm^3), t—homogenization temperature (˚C), and A, B, C—a function of salinity.

Here, $A = 0.993531 + 8.72147 \times 10^{-3} \times S - 2.43975 \times 10^{-5} \times S^2$,
$B = 7.11652 \times 10^{-5} - 5.2208 \times 10^{-5} \times S + 1.26656 \times 10^{-6} \times S^2$,
$C = -3.4997 \times 10^{-6} + 2.12124 \times 10^{-7} \times S - 4.52318 \times 10^{-9} \times S^2$,

TABLE 2 Microthermometry and physicochemical parameters of calcite mineral inclusions.

Sample no.	Inclusion type	Homogenization temperature (°C)	Freezing point temperature (°C)	Salinity (wt %NaCl)	Density (g/cm^3)	Pressure P(Mp)	Depth (m)
1	Gas–liquid two-phase (saline) inclusions	260	−8.5	12.28	0.89	4.30	962.34
2		256	−10.8	14.77	0.92	3.93	1014.15
3		243	−8.7	12.51	0.91	3.22	905.51
4		247	−9.7	13.62	0.92	3.42	949.54
5		270	−8.5	12.28	0.88	5.04	999.36
6		370	−8.3	12.05	0.74	19.13	1360.14
7		283	−3.2	5.26	0.79	6.50	796.87
8		370	−1.5	2.57	0.59	20.70	883.84

where Th—homogenization temperature (°C) and s—salinity (%).

Pressure and depth estimation follows the empirical equation by Shao (1988):

$T0 = 374 + 9.20 \times N$, $P0 = 219 + 26.20 \times N$, $P1 = P0 \times T1/T0$, and $H1 = P1/(300 \times 10^5)$. In the aforementioned formulas, T0 is the initial temperature (°C), P0 is the initial pressure value (10^5 Pa), T1 is the actual metallogenic temperature (°C), P1 is the metallogenic pressure value (10^5 Pa), H1 is the metallogenic depth (km), and N presents salinity of ore-forming fluid (NaCl%).

According to the aforementioned equations, the NaCl salinity of the fluid inclusions ranges from 2.57 to 14.77 wt% (NaCl equivalent). The density (ρ) of the inclusions varies from 0.59 to 0.92 g/cm^3. The pressure of inclusions varies between 3.22 and 20.70 megapascals (MPa). The estimated formation depth ranges from 796.87 m to 1,360.14 m, with the majority falling between 900 m and 1,000 m (Table 2).

4 Discussion

4.1 Formation age of kimberlite

The determination of the formation age of kimberlite primarily relies on the age of its characteristic minerals such as perovskite, phlogopite, baddeleyite, pyrope, and whole kimberlite. Various methods are used, including U–Pb analysis, Sm–Nd analysis, Ar–Ar isochron analysis, and K–Ar analysis (Table 3; Figure 7). The perovskite U–Pb system has closure temperatures of approximately 875°C–900°C, which are relatively high compared to other kimberlite minerals (Wu et al., 2010). As perovskite is less affected by late alteration and weathering (Paton et al., 2007; Yang et al., 2009), its recorded magma crystallization age is generally considered more reliable. Perovskite is believed to have originated from a single source and crystallized directly from the kimberlitic magma, reducing the complexity of interpreting mineral sources and ages (Heaman et al., 2019). Therefore, many researchers (Yang et al., 2009; Li et al., 2010; Sun et al., 2014; Sun et al., 2018) argue that perovskite U—Pb dating is the preferred method for dating kimberlites due to its statistical performance and widespread acceptance.

The intrusive age of diamond-bearing kimberlites (porphyrites) is estimated to be approximately 455 Ma but remains controversial. Wang et al. (2014) suggested that kimberlite emplacement in the area occurred during the Permian of the Paleozoic era (250–300 Ma), based on multiple constraints, including the age of emplacement strata, denudative sedimentary strata, paleomagnetism, joint structure, and isotopic dating. Chu et al. (2019) conducted LA-ICP-MS zircon U–Pb dating on diabase veins invaded by kimberlite and obtained a minimum age of 117–121 Ma, suggesting late Mesozoic Yanshanian kimberlite intrusion. Further comprehensive investigations are needed to resolve these controversies.

The Mengyin kimberlite magma is characterized by multiple intrusions (Hu, 1985), with three main intrusions identified in the Changmazhuang rock belt and five in the Xiyu rock belt. The second intrusion in the Xiyu rock belt is predominantly composed of massive limestone brecciated kimberlite. While ascending, kimberlite magma is rarely known to cause thermal effects, such as contact metamorphism, on the surrounding rocks of the breccia pipe zone or xenoliths, so kimberlite is generally considered a "cold" rock (Sun and Sun, 2021). However, the kimberlite in the Mengyin area contains a significant amount of surrounding rock xenoliths, where most of the early Paleozoic limestone has been thermally altered to marble after being trapped. No large-scale magmatic thermal events have been recorded in the area after the emplacement of kimberlite. Therefore, the age of the marble in this kimberlite can represent the final formation time of the kimberlite cooling epoch.

The U–Pb dating results indicate that the calcite found in the kimberlite matrix has an age of 383 ± 18 Ma, while the calcite in the marble has an age of 359 ± 28 Ma. The high U and P contents in the calcite from the matrix suggest a different origin compared to the marble, indicating a deep-seated source for the kimberlite. The ages of the kimberlite represent the time when it solidified, while the ages of the marble indicate the period when it was formed through thermal alteration, which is slightly later than the kimberlite matrix.

Various dating methods were used to analyze and test the kimberlite in the area, resulting in a significant amount of isotopic dating data ranging from 77 Ma to 765 Ma (Table 2). Field observations reveal that the kimberlite intruded into the Ordovician strata. No kimberlite breccia was found in the Badou

TABLE 3 List of ages of kimberlites in the Mengyin region.

Rock belt	Name of the rock mass	Lithology	Measured minerals	Analysis method	Dating(Ma)	Reference
Changma rock belt	Shengli No. 1	Pyrope coarse-grained kimberlite	Whole rock	K–Ar	634	Yang et al. (2015)
Changma rock belt	Shengli No. 1	Pyrope coarse-grained kimberlite	Whole rock	K–Ar	716	Yang et al., 2015; Lv et al., 2016
Changma rock belt	Shengli No. 1	Pyrope coarse-grained kimberlite	Phlogopite	Rb–Sr	494	Yang et al. (2015)
Changma rock belt	Shengli No. 1	Kimberlite	Phlogopite	Rb–Sr	484	Yang et al. (2015)
Changma rock belt	Shengli No. 1	Kimberlite	Phlogopite	Rb–Sr	474	Yang et al. (2015)
Changma rock belt	Shengli No. 1	Kimberlite	Perovskite	U–Pb SHIMP	457	Lu et al. (1995)
Changma rock belt	Shengli No. 1	Kimberlite	Perovskite	U–Th–Pb	480	Li (2016)
Changma rock belt	Shengli No. 1	Kimberlite	Phlogopite	Rb–Sr	485	Wang et al. (1997)
Changma rock belt	Shengli No. 1	Kimberlite	Whole rock	Rb–Sr isochron	616	Wang et al. (1997)
Changma rock belt	Shengli No. 1	Kimberlite	Whole rock + serpentine	Rb–Sr isochron	605	Wang et al. (1997)
Changma rock belt	Shengli No. 1	Kimberlite	Whole rock + matrix phlogopite	Rb–Sr isochron	560	Wang et al. (1997)
Changma rock belt	Shengli No. 1	Kimberlite	Whole rock + megacryst phlogopite	Rb–Sr isochron	573	Wang et al. (1997)
Changma rock belt	Shengli No. 1	Kimberlite	Whole rock +garnet	Rb–Sr isochron	651	Wang et al. (1997)
Changma rock belt	Shengli No. 1	Kimberlite	Pyrope	Rb–Sr isochron	633	Lv et al. (2016)
Changma rock belt	Shengli No. 1	Globular kimberlite	Whole rock	Rb–Sr isochron	644	Lu et al. (1995)
Changma rock belt	Shengli No. 1	Kimberlite	Phlogopite megacryst	Rb–Sr isochron	499	Lu et al. (1995)
Changma rock belt	Shengli No. 1	Fine-grained kimberlite	Whole rock	Rb–Sr isochron	765	Lu et al. (1995)
Changma rock belt	Shengli No. 1	Mantle-derived inclusions	Pyrope	Sm–Nd	550	Lv et al. (2016)
Changma rock belt	Hongqi No. 1	Kimberlite	Pyrope	Sm–Nd	625	Lv et al. (2016)
Changma rock belt	Hongqi No. 1	Fine-grained kimberlite	Whole rock	Sm–Nd	567	Lv et al. (2016)
Changma rock belt	Hongqi No. 1	Pyrope coarse-grained kimberlite	Phlogopite	K–Ar	554	Yang et al. (2015)
Changma rock belt	Hongqi No. 1	Pyrope coarse-grained kimberlite	Phlogopite	K–Ar	530	Yang et al. (2015)
Changma rock belt	Hongqi No. 1	Pyrope coarse-grained kimberlite	Phlogopite	K–Ar	476	Yang et al. (2015)
Changma rock belt	Hongqi No. 1	Pyrope coarse-grained kimberlite	Phlogopite	K–Ar	455	Yang et al. (2015)
Changma rock belt	Hongqi No. 1	Fine-grained kimberlite	Whole rock	Sm–Nd	702	Lv et al. (2016)

(Continued on following page)

TABLE 3 (*Continued*) List of ages of kimberlites in the Mengyin region.

Rock belt	Name of the rock mass	Lithology	Measured minerals	Analysis method	Dating(Ma)	Reference
Changma rock belt	Hongqi No. 2	Fine-grained kimberlite	Whole rock	Sm–Nd	486	Lv et al. (2016)
Changma rock belt	Hongqi No. 3	Porphyritic kimberlite	Whole rock	Sm–Nd	455	Lv et al. (2018)
Changma rock belt	Hongqi No. 4	Porphyritic kimberlite	Whole rock	Sm–Nd	375	Lv et al. (2016)
Changma rock belt	Shengli No. 1	Kimberlite	Perovskite	U–Pb	457	Lv et al. (2016)
Changma rock belt	Shengli No. 1	Kimberlite	Pyrope	Sm–Nd	633	Lv et al. (2016)
Changma rock belt	Shengli No. 1	Mantle-derived inclusions	Pyrope	Sm–Nd	550	Lv et al. (2016)
Changma rock belt	Shengli No. 1	Kimberlite	Phlogopite	Ar–Ar isochron	466.3	Zhang et al. (2007)
Changma rock belt	Shengli No. 1	Kimberlite	Phlogopite	Ar–Ar isochron	464.9	Zhang et al. (2007)
Changma rock belt	Hongqi No. 1	Kimberlite	Pyrope	Sm–Nd	625	Lv et al. (2016)
Xiyu rock belt	Hongqi No. 6	Phlogopite coarse-grained kimberlite	Whole rock	K–Ar	81	Yang et al. (2015)
Xiyu rock belt	Hongqi No. 6	Phlogopite coarse-grained kimberlite	Whole rock	K–Ar	88	Yang et al. (2015)
Xiyu rock belt	Hongqi No. 6	Phlogopite coarse-grained kimberlite	Whole rock	K–Ar	77	Yang et al. (2015)
Xiyu rock belt	Hongqi No. 6	Phlogopite coarse-grained kimberlite	Brown mica	K–Ar	484.6	Lv et al. (2016)
Xiyu rock belt	Hongqi No. 2	Kimberlite	Pyrope	Sm–Nd	461	Lv et al. (2016)
Xiyu rock belt	Hongqi No. 6	Porphyritic kimberlite	Whole rock	Sm–Nd	619	Zhu and Mao (1991)
Xiyu rock belt	Hongqi No. 6	Kimberlite	Whole rock	Sm–Nd	375	Lv et al. (2016)
Xiyu rock belt	Hongqi No. 2	Kimberlite	Pyrope	Sm–Nd	461	Lv et al. (2016)
Poli rock belt		Phlogopite-bearing kimberlite	Whole rock	K–Ar	371.8	Lv et al. (2016)
Poli rock belt		Phlogopite-bearing coarse-grained kimberlite	Whole rock	K–Ar	233.8	Chu et al. (2019)
Poli rock belt		Phlogopite-bearing coarse-grained kimberlite	Whole rock	K–Ar	379	Chu et al. (2019)
Poli rock belt		Kimberlite	Whole rock	Sm–Nd	479	Chu et al. (2019)
Xiyu rock belt		Kimberlite	Marble	U–Pb	332	This study
Xiyu rock belt		Kimberlite	Calcite	U–Pb	366	This study
Changma rock belt	Shengli No. 1	Kimberlite	Perovskite	U–Pb	470	Yang et al. (2009)

Formation, which is the uppermost stratum of the Ordovician, indicating that the kimberlite formed after the diagenesis of the Ordovician strata. The ages of the Ordovician Majiagou Group range from 485.4 ± 1.9 Ma to 453.0 ± 0.7 Ma (Du et al., 2019; Fan et al., 2021). Therefore, the formation age of the kimberlite should be later than 485.4 ± 1.9 Ma, after eliminating ages before 485 Ma. The remaining ages can be roughly divided into three intervals: 484.6–455 Ma, 379–332 Ma, and 233–77 Ma. In the region, the Silurian and Devonian strata are absent, and no contact relationship between the kimberlite and the strata above the Majiagou Formation (Carboniferous–Permian) has been found (Song et al., 2020). Additionally, only four whole-rock K–Ar ages exist within the interval of 233–77 Ma, which are mixed ages with low credibility. Furthermore, there is limited geological evidence to

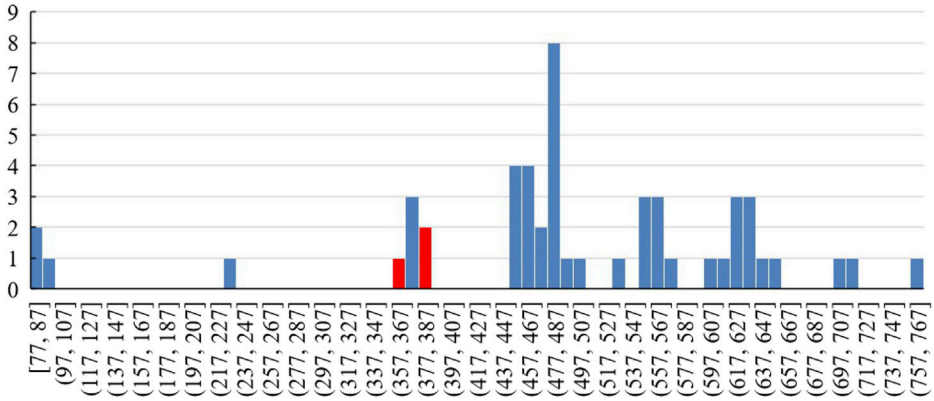

FIGURE 7
Age histograms of kimberlite in the Mengyin region.

support the formation of kimberlite during this stage, making it unlikely that the kimberlite formed at 233 Ma and beyond. Therefore, it is proposed that there were two episodes of kimberlite eruption, with the first one occurring approximately 455 Ma in the Late Ordovician and the second one ending approximately 366 Ma.

In summary, one stage of kimberlite cooling took place during the Late Devonian period (383 ± 18 Ma). Considering previous research findings, the Mengyin area witnessed two periods of kimberlite eruption: one during the Late Ordovician in the Paleozoic and another in the Late Devonian. Subsequently, the partial limestone xenoliths within the kimberlite underwent thermal metamorphism, resulting in the formation of marble, which occurred until approximately 359 ± 28 Ma. The thinning of the lithosphere in this region is believed to have occurred after the Devonian period.

Yin et al. (2005) extensively investigated the temperature, pressure, and depth conditions during diamond formation. They conducted analyses using techniques such as CL (cathode luminescence), FTIR (Fourier transform infrared reflection), and laser Raman on diamond samples from the Shengli No.1 rock pipe in Mengyin, Shandong Province. The findings indicated that most diamonds exhibited uniform CL colors, except for some samples that showed flat growth color bands under CL. This suggests that the diamond growth process was continuous and not subjected to significant dissolution or melting. By analyzing the Raman shift of olivine inclusions within the diamonds, the pressure in the source areas was estimated to be 4.6 GPa, 5 GPa, and 5.5 GPa, with corresponding formation depths for the Mengyin diamonds of 152 km, 165 km, and 181 km. These depths are close to the bottom of the lithosphere, indicating that the lithosphere's thickness during diamond formation was between 150 and 180 km. In contrast, the temperature, pressure, and depth conditions during the kimberlite eruption have not been extensively studied. In the present investigation, a comprehensive study of fluid inclusions in calcite from the kimberlite matrix and xenolithic marble was conducted to determine the temperature, pressure, and consolidation depth during a later kimberlite eruption. The analysis revealed that the temperature during the late eruption ranged from 243°C to 370°C, with a salinity ranging 2.57%–14.77% (NaCl) and pressure ranging 3.22–20.70 MPa. The formation depth was mainly estimated to be between 900 and 1,000 m, indicating that the denudation depth from the time of formation (Late Devonian) to the present is approximately 900–1,000 m. Furthermore, the denudation rate, or the rate of upward movement, from the Late Devonian to the present was estimated to be 3 m/Ma.

5 Conclusion

1) The U–Pb dating results of calcite from the Xiyu kimberlite matrix in the Mengyin area yielded an age of 383 ± 18 Ma (MSWD = 6.6), with average U and Pb contents of 4.618×10^{-6} and 4.468×10^{-6}, respectively. These age data are reliable and indicate the occurrence of a kimberlite eruption in the Mengyin area during the Late Devonian period. The *in situ* U–Pb dating age of calcite from the xenolithic marble in the kimberlite was determined to be 359 ± 28 Ma (MSWD = 6.9), with average U and Pb contents of 0.327×10^{-6} and 1.158×10^{-6}, respectively. Although the U and Pb contents are relatively low and the data quality is somewhat poor, the age value remains credible, representing the thermal alteration of kimberlite limestone xenoliths to form marble at the end of the Late Devonian.
2) It is likely that two periods of kimberlite eruption occurred in the Mengyin area, namely, during the Late Ordovician and the Late Devonian, possibly extending until the end of the Late Devonian. This suggests that the thinning of the lithosphere first took place after the Late Devonian period.
3) The analysis of fluid inclusions in calcite from the kimberlite xenolithic marble reveals important information about temperature, salinity, pressure, and formation depth. The temperature range is estimated to be between 243°C and 370°C, with salinity ranging 2.57%–14.77% (NaCl) and pressure ranging 3.22–20.70 MPa. The main formation depth is determined to be approximately 900–1,000 m, and the total denudation depth from the Late Devonian to the present is also estimated to be 900–1,000 m. Additionally, the overall rate of crustal ascent is calculated to be 3 m/Ma(Cohen et al., 2013, Du et al., 2020, Wang, 2016, Zhang et al., 2011).

Data availability statement

The original contributions presented in the study are included in the article/Supplementary Material; further inquiries can be directed to the corresponding author.

Author contributions

Conceptualization, RT, HW, and JT; Methodology, RT, HW, JT, and WS; Writing—original draft preparation, all authors; Writing—review and editing, RT, HW, and JT; Supervision, RT and HW; Funding acquisition, HW and WS. All authors have read and agreed to the submitted version of the manuscript.

Funding

This research was jointly supported by the General Project of Natural Science Foundation of Shandong Province (ZR2020MD030 and ZR2021MD052), the Science and Technology Innovation Cultivation Program of Shandong Academy of Geological Sciences (PYJH202102), and the Youth Fund from Natural Science Foundation of Shandong Province (ZR2020QD029).

Conflict of interest

The authors declare that the research was conducted in the absence of any commercial or financial relationships that could be construed as a potential conflict of interest.

Publisher's note

All claims expressed in this article are solely those of the authors and do not necessarily represent those of their affiliated organizations, or those of the publisher, the editors, and the reviewers. Any product that may be evaluated in this article, or claim that may be made by its manufacturer, is not guaranteed or endorsed by the publisher.

References

Bodnar, R. J. (1983). A method of calculating fluid inclusion volumes based on vapor bubble diameters and P-V-T-X properties of inclusion fluids. *Fluids Econ. Geol.* 78, 535–542. doi:10.2113/gsecongeo.78.3.535

Boyd, F. R., and Gurney, J. J. (1986). Diamonds and the african lithosphere. *Science* 232 (4749), 472–477. doi:10.1126/science.232.4749.472

Cai, Y. C., Fan, H. R., Hu, F. F., Yang, K. F., Lan, T. G., Yu, H., et al. (2011). Ore-forming fluids stable isotope and mineralizing age of the Hu bazhuang gold deposit Jiaodong Peninsula of eastern China. *Acta Petrol. Sin.* 27 (5), 1341–1351.

Chen, Y. M., Yang, Z. J., Huang, S. S., Lei, X. Y., Li, X. X., and Zeng, X. (2018). Microfabrics of perovskites in the menyin kimberlites and their geological implications. *Bull. Mineralogy, Petrology Geochem.* 37 (4), 1–10.

Chu, Z. Y., Wang, W. D., Lv, Q., Kang, C. X., and Wang, S. X. (2019). The formation age of the kimberlite zone in Poli area of Mengyin, Shandong Province: Zircon U-Pb dating data of diabase. *Geol. Bull. China* 38 (1), 44–50.

Cohen, K. M., Finney, S. C., Gibbard, P. L., and Fan, J.-X. (2013). The ICS international chronostratigraphic chart. *Episodes* 36, 199–204. doi:10.18814/epiiugs/2013/v36i3/002

Du, S. X., Liu, F. C., Chen, J., Gao, L. M., Song, X. S., Chen, C., et al. (2019). The cretaceous- paleocene biostratigraphy and boundary in the pingyi basin, Shandong province. *Acta Geol. Sin.* 93 (8), 1831–1848.

Du, Z. Z., Cheng, Z. Z., Yao, X. F., et al. (2020). 40Ar-39Ar age of altered potash feldspar of xiejiagou gold deposit in jiaodong and its geological significance. *J. Jilin Univ. (Earth Sci. Ed.* 50 (5), 1570–1581.

Giuliani, A., Phillips, D., Kamenetsky, V. S., and Goemann, K. (2016). Constraints on kimberlite ascent mechanisms revealed by phlogopite compositions in kimberlites and mantle xenoliths. *Lithos* 240-243, 189–201. doi:10.1016/j.lithos.2015.11.013

Haas, J. L. (1970). An equation for the density of vapor-saturated NaCl-H2O solutions from 75 degrees to 325 degrees C. *Am. J. Sci.* 269 (5), 489–493. doi:10.2475/ajs.269.5.489

Haggerty, S. E. (1986). Diamond Genesis in a multiply-constrained model. *Nature* 320 (6057), 34–38. doi:10.1038/320034a0

Heaman, L. M., Kjarsgaard, B. A., and Creaser, R. A. (2003). The timing of kimberlite magmatism in North America: Implications for global kimberlite Genesis and diamond exploration. *Lithos* 71 (2), 153–184. doi:10.1016/j.lithos.2003.07.005

Heaman, L. M., Phillips, D., and Pearson, G. (2019). Dating kimberlites: Methods and emplacement patterns through time. *Elements* 15 (6), 399–404. doi:10.2138/gselements.15.6.399

Hu, S. Y. (1985). The forming temperatures and pressures for the Mengyin kimberlites. *Geology of Shandong* 1 (1), 79–84. (in Chinese with English Abstract).

Jin, Z. K., Liu, Z. R., and Shi, Z. R. (1999). Types of fault structures and their formation mechanisms in the Western Shandong Province. *J. Univ. Petroleum, China* 23 (5), 1–5.

Li, Q. L., Li, X. H., Liu, Y., Wu, F. Y., Yang, J. H., and Mitchell, R. H. (2010). Precise U-Pb and Th-Pb age determination of kimberlitic perovskites by secondary ion mass spectrometry. *Chem. Geol.* 269 (3-4), 396–405. doi:10.1016/j.chemgeo.2009.10.014

Liu, J. T. (2002). Study on primary diamond ore-forming future in Shandong province. *Geol. Shandong* 18 (3-4), 100–104.

Lu, F. X. (2008). Kimberlite and diamond. *Chin. J. Nat.* 30 (2), 63–66.

Lu, F. X. (2010). Multiple-geological events of ancient lithospheric mantle beneath North China craton: As inferred from peridotite xenoliths in kimberlite. *Acta Petrol. Sin.* 26 (11), 3177–3188.

Lu, F. X., Zhao, L., Deng, J. F., and Zheng, J. P. (1995). The discussion on the ages of kimberlitic magma activity in north China platform. *Acta Pet. Sin.* 11 (4), 365–374.

Lu, F. X., Zheng, J. P., and Chen, M. H. (1998). Discussion on formation condition of diamonds. *Earth Sci. Front.* 5 (3), 125–131.

Luo, S. X., Ren, X. R., and Zhu, Y. (1999). *Diamond geology of Shandong*. Jinan, China: Shandong Science and Technology Publishing House, 1–131.

Lv, Q., and Ge, Y. J. (2016). Study on age dating methods and age dating samples of kimberlite. *Shandong Land Resour.* 32 (10), 12–15.

Paton, C., Hellstrom, J., Paul, B., Woodhead, J., and Hergt, J. (2011). Iolite: Freeware for the visualisation and processing of mass spectrometric data. *J. Anal. Atomic Spectrom.* 26 (12), 2508–2518. doi:10.1039/c1ja10172b

Paton, C., Hergt, J. M., Phillips, D., Woodhead, J. D., and Shee, S. R. (2007). New insights into the Genesis of Indian kimberlites from the Dharwar Craton via *in situ* Sr isotope analysis of groundmass perovskite. *Geology* 35 (11), 1011–1014. doi:10.1130/g24040a.1

Potter, W., Clynne, M. A., and Brown, L. (1978). Freezing point depression of aqueous sodium chloride solutions. *Econ. Geol.* 73 (2), 284–285. doi:10.2113/gsecongeo.73.2.284

Sheng, X. Y. (2004). Diamond prospecting deserved in persistence: Viewpoints for the anomaly of diamond in East Guizhou 21 (4), 234–239. (in Chinese with English Abstract).

Shao, J. L. (1988). *Mineralogy of gold ore prospecting*. Beijing, China: China University of Geosciences Press, 1–158.

Song, M. C., Xu, J. X., and Wang, P. C. (2009). *Tectonic framework and tectonic evolution of the shandona Province*. Shandong, China: Geology Press, 114.

Song, M. C., Yu, X. S., Song, Y. X., Xiao, B. J., Zhou, D. S., Gao, C. S., et al. (2020). Types, sources, and regional crust-mantle evolution background of diamonds in the Western Shandong Province. *Acta Geol. Sin.* 94 (9), 2606–2625.

Sun, J., Liu, C. Z., Tappe, S., Kostrovitsky, S. I., Wu, F. Y., Yakovlev, D., et al. (2014). Repeated kimberlite magmatism beneath Yakutia and its relationship to Siberian flood volcanism: Insights from *in situ* U-Pb and Sr-Nd perovskite isotope analysis. *Earth Planet. Sci. Lett.* 404, 283–295. doi:10.1016/j.epsl.2014.07.039

Sun, J., Tappe, S., Kostrovitsky, S. I., Liu, C. Z., Skuzovatov, S. Y., and Wu, F. Y. (2018). Mantle sources of kimberlites through time: A U-Pb and Lu-Hf isotope study of zircon megacrysts from the siberian diamond fields. *Chem. Geol.* 479, 228–240. doi:10.1016/j.chemgeo.2018.01.013

Sun, J. X., and Sun, J. (2022). Review of kimberlite dating methods. *Bull. Mineralogy Petrology Geochem.* 41 (1), 175–196.

Wang, X. F. (2016). Orsovocoan tectonic-paleogegraphy in South China and chrono and biostratigraphic divison and correlation. *Earth Sci. Front.* 26 (6), 253–267.

Wang, Y., Ling, W. L., and Lu, F. X. (1997). *Geol. Sci. Technol. Inf.* 16 (3), 9–12.

Wang, Z. B., Cao, H. C., Li, D. P., Bian, Q., Wang, Q. J., and Yang, B. (2015). Mineralization and prospecting significance of kimberlite deposit in fangshan area of Shandong province. *Shandong Land Resour.* 31 (5), 1–6.

Wang, Z. B., Lv, Q., Ge, Y. J., Wang, Q. J., and Peng, J. (2013). Diversity of culturable root-associated/endophytic bacteria and their chitinolytic and aflatoxin inhibition activity of peanut plant in China. *Shandong Land Resour.* 29 (10-11), 1–10. doi:10.1007/s11274-012-1135-x

Wang, Z. B., and Wang, Q. J. (2014). Analysis on regional geological background and metallogenic predication of diamond mineralization in eastern margin of north China plate. *Shandong Land Resour.* 30 (10), 8–14+20.

Wu, F. Y., Yang, Y. H., Mitchell, R. H., Li, Q. L., Yang, J. H., and Zhang, Y. B. (2010). *In situ* U-Pb age determination and Nd isotopic analysis of perovskites from kimberlites in southern Africa and Somerset Island, Canada. *Lithos* 115 (1-4), 205–222. doi:10.1016/j.lithos.2009.12.010

Yang, B., Ma, X. X., Tang, L. L., Lu, W. Q., and Sun, X. Z. (2015). Discussion on forming age of primary diamond ore in Mengyin area of Shandong province. *Shandong Land Resour.* 31 (4), 19–21.

Yang, P., Wu, G., Nuriel, P., Nguyen, A. D., Chen, Y., Yang, S., et al. (2021). *In situ* LA-ICPMS UPb dating and geochemical characterization of fault-zone calcite in the central Tarim Basin, northwest China: Implications for fluid circulation and fault reactivation. *Chem. Geol.* 568, 120125–125. doi:10.1016/j.chemgeo.2021.120125

Yang, Y. H., Wu, F. Y., SimonWildeLiu, A. X. M., Zhang, Y. B., Xie, L. W., Yang, J. H., et al. (2009). *In situ* perovskite Sr–Nd isotopic constraints on the petrogenesis of the Ordovician Mengyin kimberlites in the North China Craton. *Chem. Geol.* 264, 24–42. doi:10.1016/j.chemgeo.2009.02.011

Yang, Z. J., Huang, S. S., Chen, Y. M., Lei, X. Y., Li, X. X., and Zeng, X. (2018). Characteristics and their geological significances of spinel minerals of kimberlite in Mengyin, Shandong province. *Bull. Mineralogy, Petrology Geochem.* 37 (2), 168–179+371.

Yin, Z. W., Lu, F. X., Chen, M. H., and Xu, H. Y. (2005). Ages and environments of formation of diamonds in Mengyin county, Shandong province. *Earth Sci. Front.* 12 (4), 614–621.

Zhang, H. F., and Yang, Y. H. (2007). Emplacement age and Sr-Nd-Hf isotopic characteristics of the diamondiferous Kimberlite from the eastern North China Craton. *Acta Petrol. Sin.* 23 (2), 285–294.

Zhang, P. Q. (2006) Origin of kimberlitic pipes in Shandong Province. PhD thesis. Beijing, China: China University of Geosciences, 24–29.

Zhang, Z. Q., Liu, S. C., Du, S. X., Shan, W., Cheng, G. S., and Zhang, S. K. (2011). Determination opinions on stratigraphic division and correlation in Shandong province. *Shandong Land Resour.* 27 (09), 1–9.

Zhao, X. F. (2019). A study of diamond indicative minerals in the depth and periphery of Xiyu, Mengyin County, Shandong Province: Metallogenic properties of kimberlite predicted by diamond indicating minerals. *Geol. Bull. China* 38 (1), 121–131.

Zhou, Q., Wu, F. Y., Chu, Z. Y., Yang, Y. H., Sun, D. Y., and Ge, W. C. (2007). Sr-Nd-Hf-Os isotopic charaeterizaitons of the Jiaohe Peridotite xenoilhts in Jilin Province and constraints on the lithosPheric mantle age in northeasetrn China. *Aeate Petrol. Sin.* 23 (6), 1269–1280.

Zhu, Y., and Mao, Z. H. (1991). Preliminary investigation on geochemical property of kimberlite isotope in Shandong. *Geol. Sci. Technol. Inf.* 10 (S1), 77–84.